Journal of Power Sources 195 (2010) 1256–1262

Contents lists available at ScienceDirect

Journal of Power Sources

journal homepage: www.elsevier.com/locate/jpowsour

Multiwall carbon nanotube-poly(4-styrenesulfonic acid) supported polypyrrole/manganese oxide nano-composites for high performance electrochemical electrodes

Raj Kishore Sharma[a], Ajay Karakoti[c], Sudipta Seal[a,c], Lei Zhai[a,b,*]

[a] NanoScience Technology Center, University of Central Florida, 12424 Research Parkway, Suit 400, Orlando, FL 32826, USA
[b] Department of Chemistry, University of Central Florida, 4000 Central Florida Blvd, Orlando, FL 32816, USA
[c] Advanced Materials Processing Analysis Center, Mechanical, Materials and Aerospace Engineering, University of Central Florida, 4000 Central Florida Blvd, Orlando, FL 32816, USA

ARTICLE INFO

Article history:
Received 15 July 2009
Received in revised form 28 August 2009
Accepted 31 August 2009
Available online 4 September 2009

Keywords:
Supercapacitor
Rate capability
Polypyrrole
MnO_2 electrochemical electrode

ABSTRACT

Poly(4-styrenesulfonic acid) (PSS) dispersed multiwall carbon nanotubes (MWCNTs) are used as a support for polypyrrole (PPy)/MnO_2 in a supercapacitor electrode. Synergetic interaction between polypyrrole and MnO_2 significantly improves the electrical properties and the mechanical stability of the electrode that yields high rate capability. The ($-SO_3^-$) surface functionalities on MWCNT-PSS facilitate an ordered growth, and the molecular level dispersion of MnO_2 in PPy matrix enhances the electrode performance. As an electrochemical electrode the MWCNT-PSS/PPy:MnO_2 nano-composite exhibits ~268 F g^{-1} specific capacitance at 5 mV s^{-1}. The excellent rate capability and stability of the electrode is demonstrated by only 7% fade in the specific capacity at 100 mV s^{-1} (compared to the available capacity at 5 mV s^{-1}) and 10% fade in the same after 5000 CV cycles. Specific capacitance of PPy:MnO_2 component in the nano-composite is as high as 412 F g^{-1} in 0.5 M Na_2SO_4 electrolyte. Electrical conductivity of the MWCNT-PSS/PPy nano-composite is significantly improved upon inclusion of MnO_2 in molecular level dispersion.

1. Introduction

Supercapacitors, depending on electrode materials, store charges in electrical double-layers, through faradaic process or by the combination of both [1]. Faradaic process in pseudo-capacitive materials (i.e. conducting polymers and metal-oxides) has been extensively investigated [2–5]. Despite demonstrating great potential as efficient charge storage materials, conducting polymers and metal-oxides suffer from mechanical instability and poor electrical conductivity that inhibits their application in supercapacitor devices. On the other hand, carbon materials constitute double-layer capacitors with high rate capability and good electrical conductivity. Carbon in its dispersed and conducting form is most widely used commercial material for supercapacitors, and also used to improve the electrical conductivity and mechanical stability of pseudo-capacitive materials [6–8]. Among the carbon materials, carbon nanotubes (CNTs) offer a unique mesoporous network with high accessible surface area, excellent electrical conductivity, good mechanical properties and chemical stability [9]. The effective utilization of CNTs depends strongly on the ability to disperse nanotubes homogeneously in solvents down to individual tube level [10]. Further studies on the preparation of pseudo-capacitive material/CNT composites show that the loading of pseudo-capacitive materials on CNTs or assembling the composite on current collector develops a high contact resistance [11]. Dispersion, surface activation or ordered assembling of CNTs have been investigated to achieve low contact resistance and high surface area [12–14]. Surface modification by coating a conducting polymer layer increases the CNT electrochemical performance [13]. Studies on conducting polymer/CNT electrodes suggest a synergetic action that significantly improves the electrode performance [15–17].

In this work, for the first time, we report a novel and cost-effective fabrication of CNT/polypyrrole (PPy) nano-composite on poly(4-styrenesulfonic acid) (PSS) dispersed multiwall carbon nanotubes (MWCNTs). PSS not only stabilizes MWCNT suspension but also provides charged groups to facilitate an ordered and uniform growth of pseudo-capacitive materials around MWCNTs through electrostatic attractions [18]. Unlike the reported processes that disperse or grow CNTs in aligned arrays, our synthetic process is based on a simple wet chemical reaction with individual CNTs, providing a cost-effective and efficient approach to fabricate nano-composite electrodes. It is demonstrated that the MWCNT-PSS/PPy

* Corresponding author at: NanoScience Technology Center and Department of Chemistry, University of Central Florida, 12424 Research Parkway, Suit 400, Orlando, FL 32826, USA.
E-mail address: lzhai@mail.ucf.edu (L. Zhai).

0378-7753/$ – see front matter © 2009 Elsevier B.V. All rights reserved.
doi:10.1016/j.jpowsour.2009.08.093

nano-composite is highly capacitive, and the addition of MnO_2 to the PPy matrix on MWCNT-PSS leads to high rate capability and excellent performance.

2. Experimental

MWCNTs (diameter: 10–20 nm, length: 5–20 μm) were purchased from Nanolab (Newton MA). 10 mg MWCNTs were dispersed in 10 ml DI water using 0.3 ml, 18 wt% PSS. During the sonication, PSS wrapped around and formed a layer on MWCNT surface, which stabilized the nanotubes in water through charge repulsion [18]. The negatively charged PSS layer on MWCNTs attracted pyrrole and metal ions, and served as templates for subsequent nano-structure formation. Interaction of growing nuclei with large number of surface sites ($-SO_3^-$) facilitated the material to grow in nano-dimensions, and retarded inter-particle agglomeration. Oxidation of pyrrole using $KMnO_4$ was carried out to produce PPy:MnO_2 nano-composite. In order to investigate the material performance, MWCNT supported MnO_2 and PPy were also synthesized separately using $Mn(CH_3COO)_2{\cdot}4H_2O$ and $KMnO_4$ for MnO_2 and $Na_2S_2O_8$ to oxidize pyrrole. MWCNT nano-composite in aqueous solutions were centrifuged and washed several times. Extracted solid nano-composite material was then mixed with 5 wt% nafion as binder and sprayed onto polished graphite plates. The deposited nano-composite films were dried for 30 min at 80 °C in air and used as electrodes. Nano-composite materials were characterized using transmission electron microscope (TEM) and field emission scanning electron microscope (FESEM). Film composition and phase structures were examined using X-ray photoelectron spectroscopy (XPS). XPS analysis was performed with the Physical Electronics Model 5400 X-ray photoelectron spectrometer using non-monochromated Mg K X-rays. Any charging shifts produced by these semiconducting samples were removed by using a binding energy scale established by fixing the C1s binding energy of the hydrocarbon part of any adventitious carbon at 284.6 eV. AugerScan software was used with most of the common features of modern XPS peak fittings. Non-linear least-square curve fitting was performed using Gaussian/Lorentzian peak shapes. Detailed quantification of selected XPS peaks was performed using this same computer program, which automatically includes well-established sensitivity factors [19]. Current–voltage characteristic of the nano-composite materials was studied in ±1 V range, and the electrode contacts were made using colloidal silver paste. Nitrogen adsorption–desorption isotherms were performed with BET sorptometer (Nova 4200, Quantachrome) using nitrogen physisorption and the pore size distribution and pore volume were calculated by BJH (Barrett–Joyner–Halenda) method from the desorption branch. The specific surface areas (S_{BET}) were calculated from the adsorption data in the relative pressure intervals from 0.05 to 0.3 using the Brunauer–Emmett–Teller (BET) method. Electrochemical characterization was carried out in three electrode electrochemical cell consisting of a platinum plate, saturated Ag/AgCl and the nano-composite coated graphite plate as counter, reference and working electrode (area: 1 cm^2), respectively with 0.5 M Na_2SO_4 as electrolyte. Performance of the prepared electrodes was studied by galvanic charge–discharge, cyclic voltametry and electrochemical impedance spectroscopy using CHI 660B electrochemical workstation.

3. Results and discussion

Fig. 1a shows the XPS surface scan spectra of MWCNT-PSS/PPy:MnO_2 nano-composite. The C1s XPS transitions are originated from the CNT-PSS and PPy matrix. Presence of manganese oxide is evidenced by manganese $Mn2p_{3/2}$ and $Mn2p_{1/2}$ peaks along with oxygen O1s XPS peaks. The Mn2p region consists of a spin orbit doublet with $Mn2p_{1/2}$ having a binding energy of 654.30 eV and $Mn2p_{3/2}$ with a binding energy of 641.75 eV which are characteristics of manganese system [3,20]. High resolution core level spectrum of MWCNT-PSS/PPy:MnO_2 nano-composite in Fig. 1b shows that $Mn2p_{3/2}$ and $Mn2p_{1/2}$ transitions center at 641.7 and 654.7 eV, respectively. Deconvoluted $Mn2p_{3/2}$ peaks at 641.71 and 643.17 eV are attributed to the presence of Mn^{4+} and Mn^{3+} oxides, respectively. These results are consistent with the reported data for Mn_3O_4 and MnO_2 [21]. Existence of Mn-oxides is also reflected in O1s core level spectra shown in Fig. 1c. Binding energy separation (~110.45 eV) between O1s oxide component peak and the $Mn2p_{3/2}$ peak for Mn(IV) is an indication of Mn–O–Mn bonding structure [20,22]. The spectrum can be deconvoluted into three components, which are related to the Mn–O–Mn bond (531.31 eV) for the tetravalent oxide, the Mn–OH bond (531.67 eV)

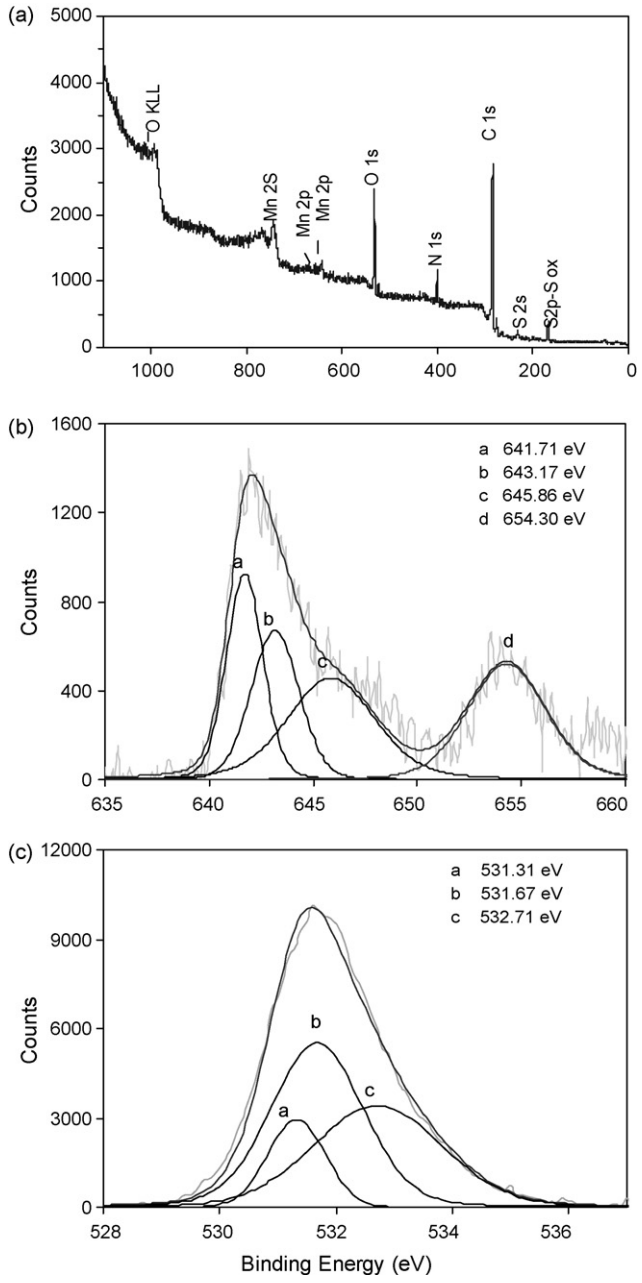

Fig. 1. XPS spectra of (a) MWCNT-PSS/PPy:MnO_2, (b) Mn2p core level XPS spectra of MWCNT-PSS/PPy:MnO_2 nano-composite, and (c) O1s core level XPS spectra and deconvoluted peak positions corresponding to Mn–O and Mn–OH.

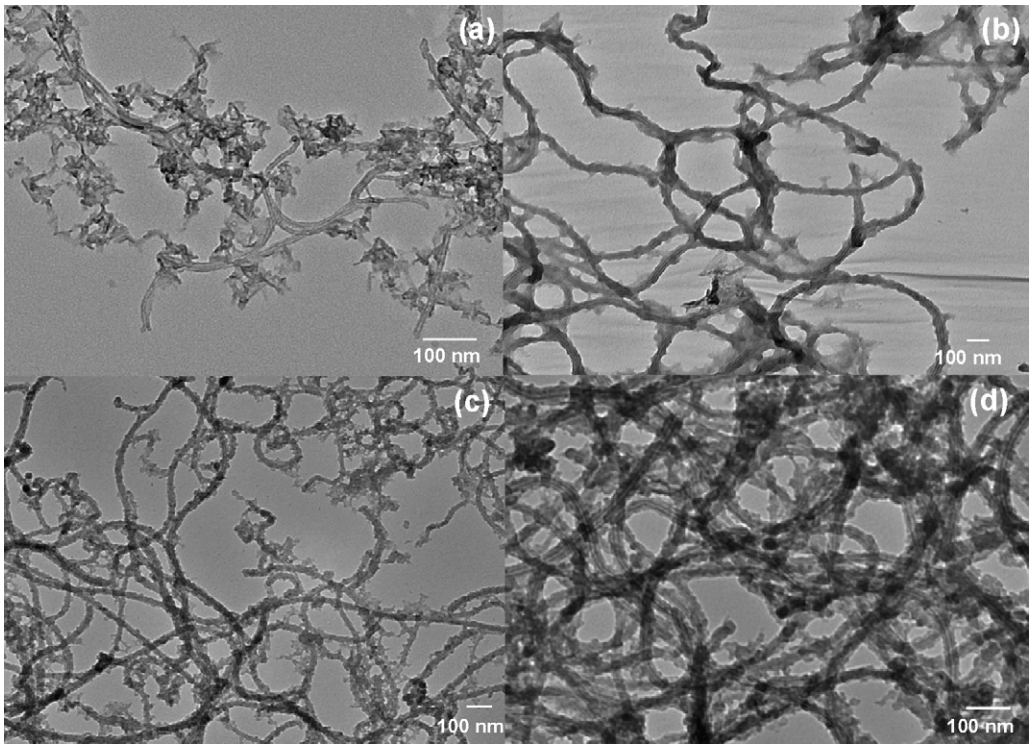

Fig. 2. TEM images of the surface microstructure of (a) MWCNT/PPy, (b) MWCNT-PSS/PPy, and (c and d) MWCNT-PSS/PPy:MnO_2 nano-composite films (scale bar = 100 nm).

for a hydrated trivalent oxide, and the H–O–H bond (532.71 eV) for residual water.

The effect of PSS on the dispersion of MWCNTs is clearly observed in Fig. 2a and b. The TEM image of MWCNT/PPy prepared without PSS (Fig. 2a) shows that PPy grows with limited interaction on MWCNTs whereas Fig. 2b depicts that a 30 nm PPy film uniformly covers the PSS dispersed MWCNT (MWCNT-PSS) surfaces (35 wt% MWCNT-PSS and 65 wt% PPy). Upon adding MnO_2 to the PPy matrix (Fig. 2c and d), the formed MWCNT-PSS/PPy:MnO_2 nano-composite (MWCNT-PSS 35 wt%, PPy 44 wt%, MnO_2 21 wt%) revealed different morphology. The uniform incorporation of nano-dimensional MnO_2 in PPy matrix is clearly demonstrated by the nano-level (2–5 nm) surface roughness in Fig. 2c and d. The high resolution TEM images of the MWCNT-PSS/PPy:MnO_2 nano-composite (corresponding to Fig. 2c and d) are shown in Fig. 3a and b. The micrographs in Fig. 2c and d show that the PPy:MnO_2 nano-composite completely and uniformly covers the MWCNT-PSS. No agglomerations caused by the bundling of MWCNTs or by the separated growth of MnO_2 and/or PPy are observed. The high resolution pictures in Fig. 3a and b support the inferences and show that the nano-composite has built ~30 nm thick uniform layer covering the MWCNT-PSS completely.

The surface area was calculated from multipoint BET while the pore size distribution was found using BJH pore size distribution from the desorption arm. The nitrogen adsorption–desorption isotherms for surface area calculations are shown in Fig. 4a. The results suggest that both the nano-composites (MWCNT-PSS/PPy and MWCNT-PSS/PPy:MnO_2) show similar typical isotherm for materials with a mixture of meso- and macro-porosity [23]. The BJH pore size distribution analysis in Fig. 4b shows a

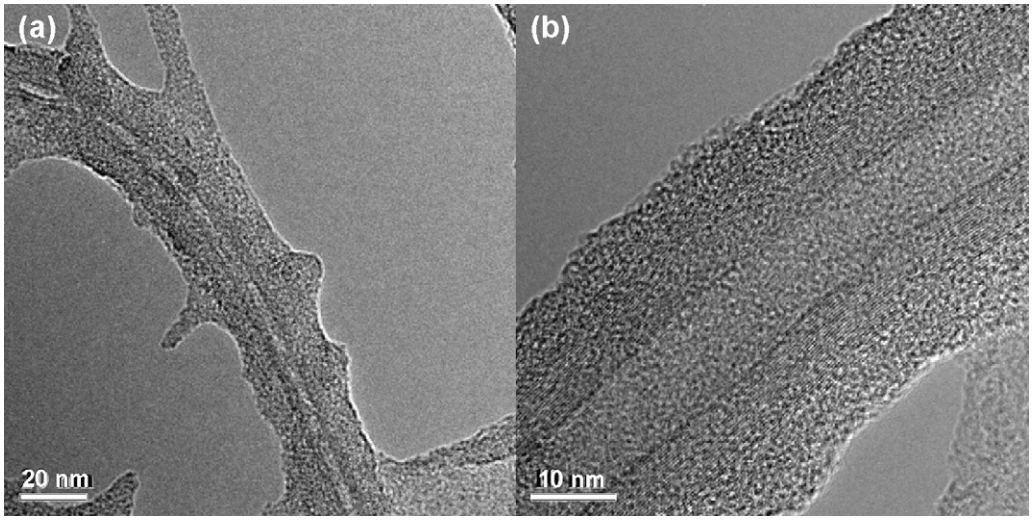

Fig. 3. High resolution TEM images of the MWCNT-PSS/PPy:MnO_2 nano-composite.

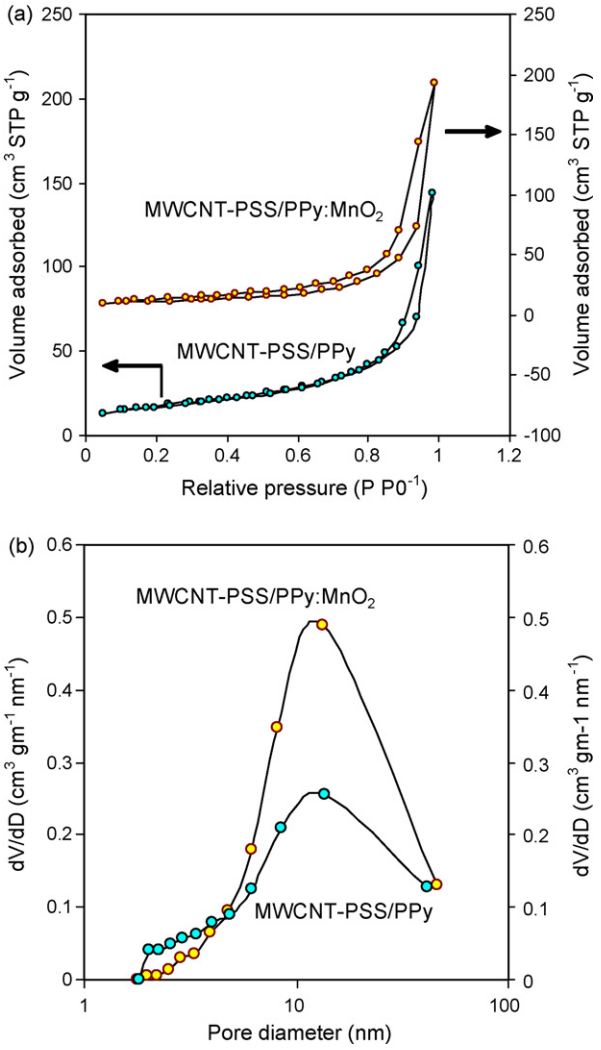

Fig. 4. Nitrogen adsorption–desorption isotherms for (a) MWCNT-PSS/PPy:MnO_2 and MWCNT-PSS/PPy nano-composites and (b) pore size distribution for both the nano-composites.

broad peak in the range of 8–50 nm for both MWCNT-PSS/PPy (pore volume—0.299 $cm^3\,g^{-1}$) and MWCNT-PSS/PPy:MnO_2 (pore volume—0.319 $cm^3\,g^{-1}$). The surface area from the multipoint BET analysis was also similar for both MWCNT-PSS/PPy:MnO_2 (57.507 $m^2\,g^{-1}$) and MWCNT-PSS/PPy (61.658 $m^2\,g^{-1}$) nano-composites. The low values of surface area are expected as the nano-composite material has completely covered the MWCNT-PSS surfaces and no pores are available from the CNT support. It is thus inferred that the surface area values and the pore size distribution observed are purely form the nano-composite materials coated over MWCNT-PSS.

FESEM micrograph of MWCNT-PSS/PPy:MnO_2 electrode in Fig. 5a shows porous morphology with high accessible area for SO_4^{2-} dopant ions from electrolyte to the pseudo-capacitive material. The cross-sectional view of MWCNT-PSS/PPy:MnO_2 nano-composite film in Fig. 5b shows that the nano-composite morphology is highly porous, enabling a large surface accessible to the electrolytic dopant ions. Electrochemical performance of the nano-composite material is evaluated by recording cyclic-voltammograms (CVs) at various scan rates. CVs recorded for MWCNT-PSS/PPy:MnO_2 nano-composite electrode in Fig. 6a show that the nano-composite has excellent rate capability. Only 7% fade in total capacity (from 5 to 100 mV s^{-1}) of MWCNT-PSS/PPy:MnO_2 electrode essentially demonstrates the high performance in comparison to 40% fade for MWCNT-PSS/PPy (Fig. 6b) and 64% fade for MWCNT-PSS/MnO_2 (Fig. 6c). The high rate capability of MWCNT-PSS/PPy:MnO_2 nano-composite (Fig. 6d) is achieved by forming interconnected PPy and MnO_2 nano-structures via a concurrent deposition of MnO_2 and PPy. Considering the microstructure in Fig. 2b, PPy completely covers the MWCNT-PSS and exhibits squarish CV at low scan rates, suggesting good capacitive performance with a small decay at higher scan rates. In contrast, the charge transfer process in MWCNT-PSS/MnO_2 nano-composite electrode in Fig. 6c, is greatly affected due to inefficient electron transfer between the MnO_2 and MWCNTs at high scan rates [16].

The charge transfer in nano-composite electrodes was studied by using electrochemical impedance spectroscopy (10 kHz to 10 mHz). Nyquist plot for MWCNT-PSS/PPy:MnO_2 nano-composite in Fig. 7a suggests that the MWCNT-PSS/PPy:MnO_2 nano-composite has very low charge transfer resistance, and capacitive process starts at 7 Hz. Compared with the diffusion limitation in the charge storage process of MWCNT-PSS/PPy in Fig. 7b, it is suggested that the presence of MnO_2 in PPy matrix (Fig. 7a) improves the accessibility of active materials to dopant ions, and leads to a higher capacitance. Nyquist plot for MWCNT-PSS/MnO_2 nano-composite electrode (Fig. 7c) shows high charge transfer resistance and a Warburg element of diffusion limitations. These results are in good agreement with the CV plots in Fig. 6. It is assumed that the sulfonate ($-SO_3^-$) modified MWCNTs provide charged sites on MWCNT surfaces that attract/bind the growing nuclei and facilitate an ordered growth of the pseudo-capacitive materials. The in-situ polymerization of pyrrole using $KMnO_4$, results in the formation of PPy:MnO_2 nano-composite with MnO_2 dispersed in PPy matrix at molecular level. Such uniform dispersion of MnO_2 in PPy matrix improves the

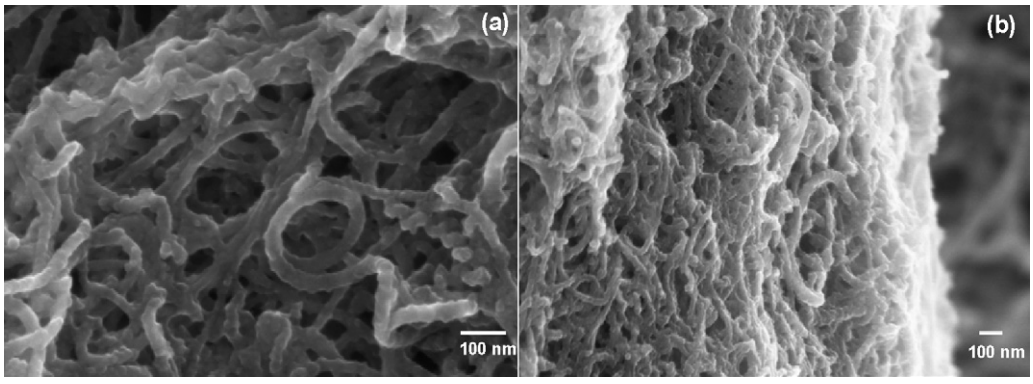

Fig. 5. Field emission electron microscopic images of (a) MWCNT-PSS/PPy:MnO_2 nano-composite film and (b) cross-sectional view of MWCNT-PSS/PPy:MnO_2 film (scale bar = 100 nm).

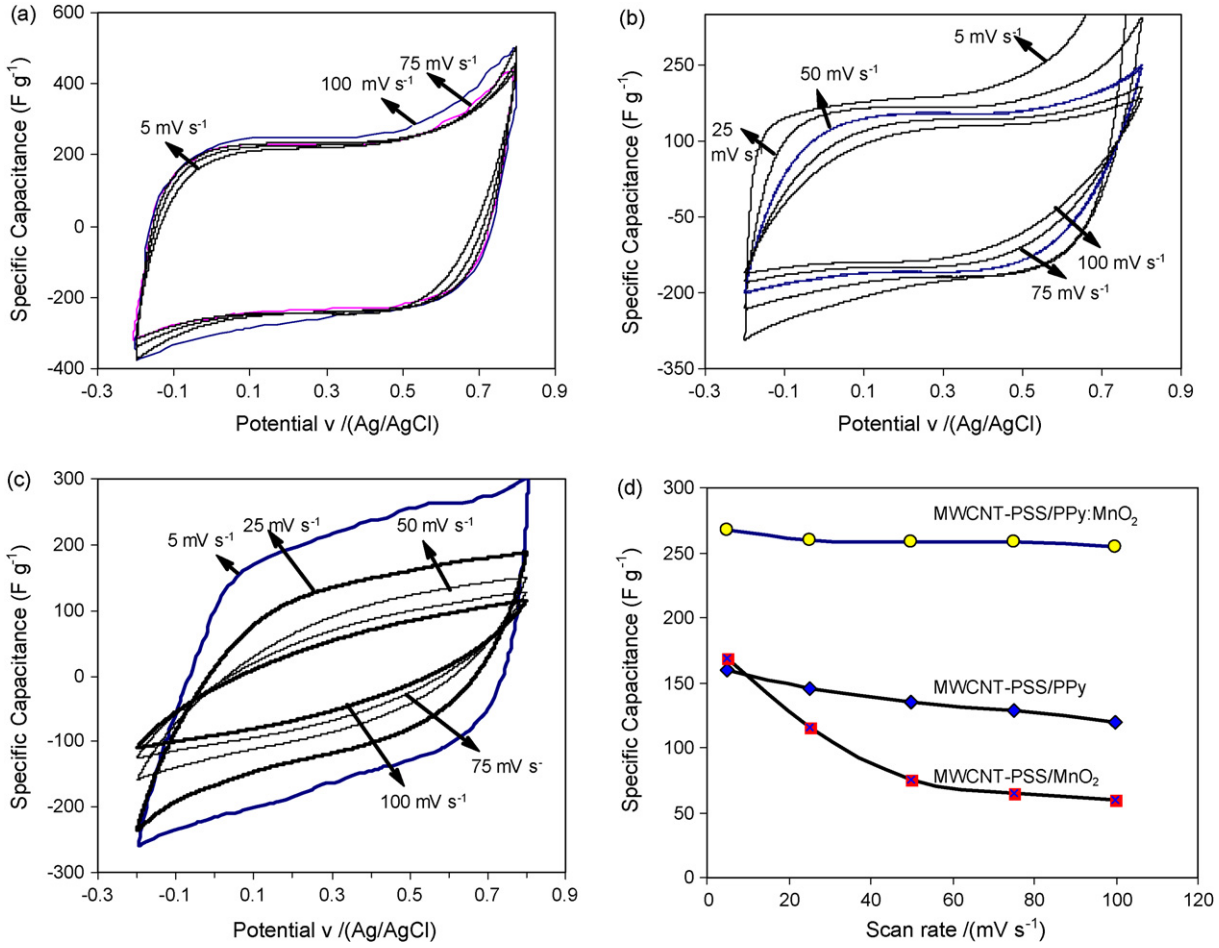

Fig. 6. Electrochemical rate capability: (a) cyclic voltammogram recorded for MWCNT-PSS/PPy:MnO_2, (b) MWCNT-PSS/PPy, (c) MWCNT-PSS/MnO_2 nano-composite electrode in 0.5 M Na_2SO_4 and (d) change in specific capacitance of the nano-composite electrodes with potential scan rate. Mass of the electrode is 1.2 mg in each case.

PPy conductivity and leads to high rate capability in MWCNT-PSS/PPy:MnO_2.

The enhancement in the conductance of PPy by incorporating MnO_2 as molecular level dispersion on MWCNT-PSS was studied using a current/voltage (I/V) measurement. Fig. 8 shows the I/V characteristics of MWCNT-PSS/PPy:MnO_2 and MWCNT-PSS/PPy nano-composite electrodes. The liner behavior suggests the ohmic properties of the materials. The calculated resistance for MWCNT-PSS/PPy:MnO_2 and MWCNT-PSS/PPy nano-composite electrode was found to be 1.56×10^6 and $1.06 \times 10^8\ \Omega$, respectively. The

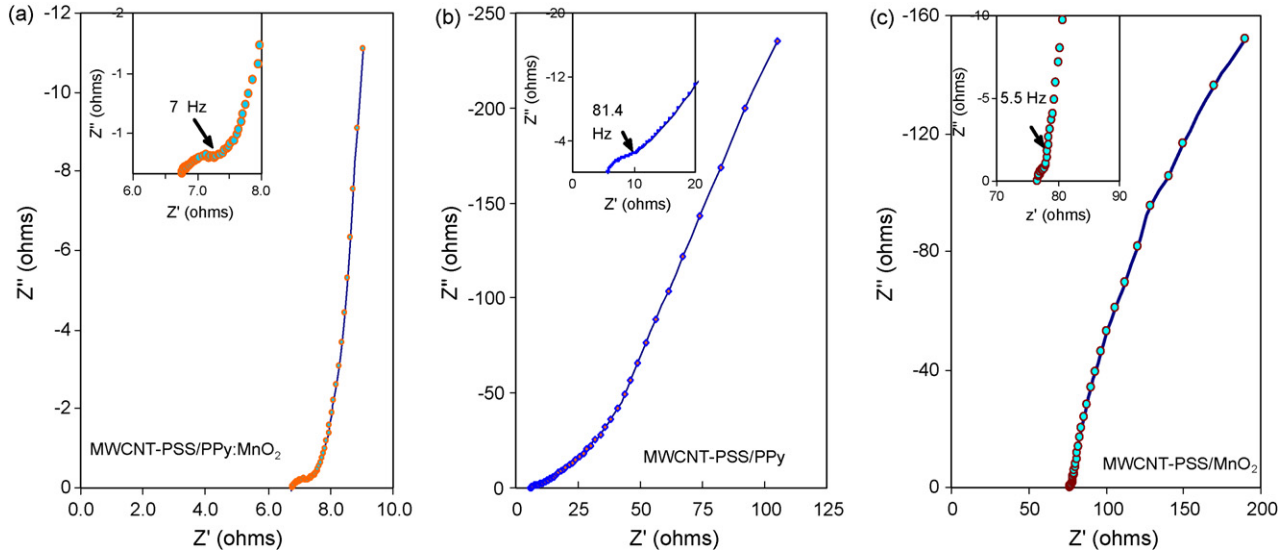

Fig. 7. Electrochemical impedance plots for (a) MWCNT-PSS/PPy:MnO_2, (b) MWCNT-PSS/PPy and (c) MWCNT-PSS/MnO_2 nano-composite electrodes, electrolyte 0.5 M Na_2SO_4.

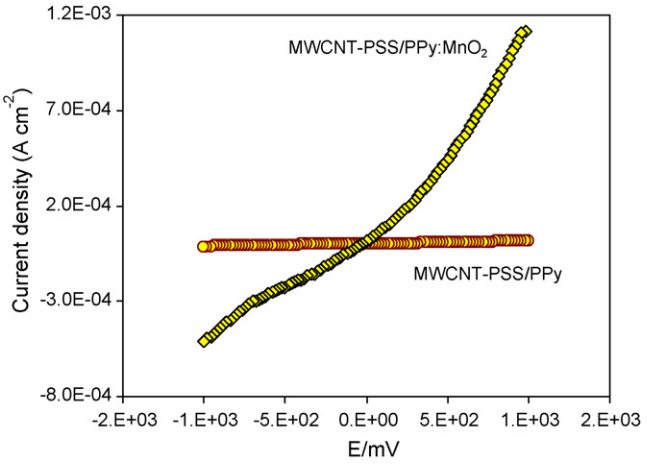

Fig. 8. *I*/*V* characteristics of MWCNT-PSS/PPy:MnO_2 and MWCNT-PSS/PPy nano-composites.

experimental data and the *I*/*V* plots in Fig. 8 show that the incorporation of MnO_2 in PPy matrix plays an important role for improving the electrical conductivity of PPy:MnO_2. It is assumed that the incorporation of MnO_2 in PPy matrix can minimize the electron shuttling along the PPy conjugated chains. Moreover, this can significantly contribute to overall conductivity of the matrix by interlinking the PPy chains and thus avoiding the inter-chain hopping and the conduction through non-conducting PPy chain ends [24].

During the reaction of pyrrol with $KMnO_4$, concurrent growth of MnO_2 with PPy generates uniform and ordered structures that lead to efficient performance in charge storage [25]. Furthermore, the improved electronic conduction by the molecular level interactions of MnO_2 and PPy results in high rate capability in electrochemical electrode. During the redox cycling, mass insertion/ejection takes place in the polymer chains, and the repetitive swelling/shrinkage causes chain defects in the polymer matrix, deteriorating the mechanical stability and electronic conduction of the electrode. The deterioration in CV performance at high scan rates in Fig. 6b supports the inference that the molecular level dispersion of MnO_2 in PPy matrix has an important effect on MWCNT-PSS/PPy:MnO_2 conductivity. It is assumed that the rate performance of MWCNT-PSS/PPy is affected by low PPy conductivity compared with PPy:MnO_2 conductivity, and the charge collection process may take place through electron hopping [21]. The poor rate performance of MWCNT-PSS/MnO_2 nano-composite electrode due to inefficient electronic conduction is explained in the earlier communication [16].

Long cycling life is an important issue for supercapacitor electrodes. The cycling life tests over 5000 CV cycles for MWCNT-PSS/PPy:MnO_2, MWCNT-PSS/PPy and MWCNT-PSS/MnO_2 electrodes were carried out. Fig. 9a shows that all the there nano-composite electrodes show a decay in available specific capacity. MWCNT-PSS/PPy:MnO_2 electrode shows a decay for the initial 1000 cycles, and for the rest 4000 cycles, the stable capacity of the electrode suggests a good cycling life. Initial decrease in the specific capacitance of electrochemical electrodes is generally observed and is attributed to the poor mechanical stability of the electrode material. The cycling life test of the rest two nano-composite electrodes shows a decrease in the specific capacity. This deterioration in the electrode performance is attributed to the dissolution of electrode material or the developed mechanical and electrical faults in the polymer chains on repetitive polymer swelling/shrinking during the charge–discharge cycles. The decay in the specific capacitance of these three nano-composite electrodes is evaluated by normalizing the maximum specific capacitance and the percentage decay is quantified. Fig. 9b shows the normalized specific capacitance in a life cycle test for 5000 CV cycles. The MWCNT-PSS/PPy:MnO_2 nano-composite exhibited a very stable cycling life with only 10% fade in specific capacity after 5000 CV cycles. Under the similar test, MWCNT-PSS/PPy and MWCNT-PSS/MnO_2 nano-composite showed much higher (i.e. 45% and 61%, respectively) decrease in the specific capacity. This observation essentially supports the MWCNT-PSS/PPy:MnO_2 nano-composite as high rate capability and excellent electrochemical performance material for supercapacitor electrodes.

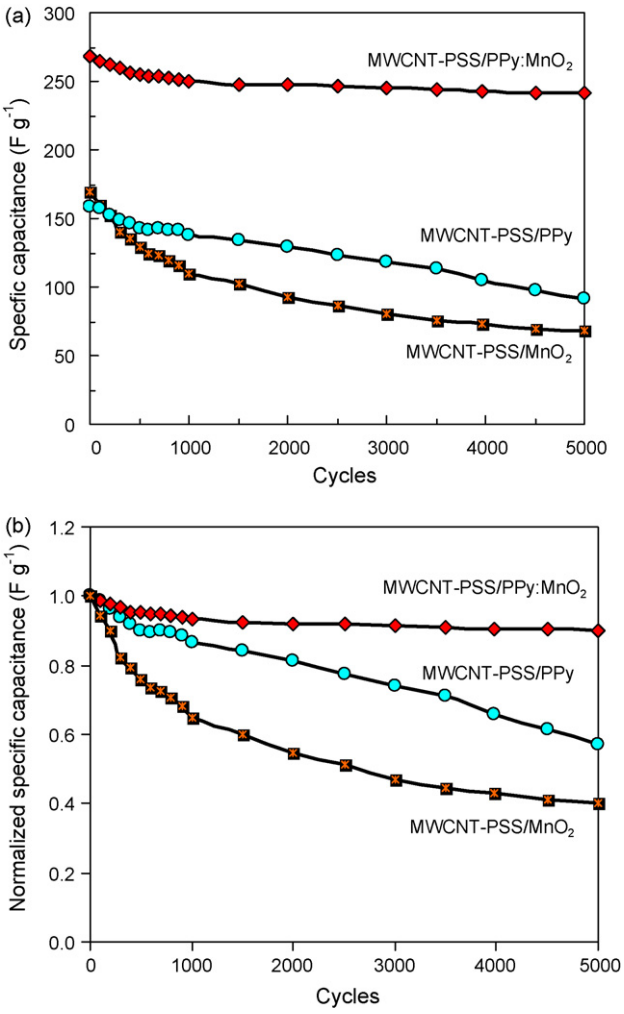

Fig. 9. Cycling life stability of MWCNT-PSS/PPy:MnO_2, MWCNT-PSS/PPy and MWCNT-PSS/MnO_2 nano-composite electrodes. (a) Decrease in specific capacitance over 5000 cycles. (b) Normalized specific capacitance.

4. Conclusion

A simple and cost-effective approach is developed to fabricate efficient MWCNT-PSS/PPy:MnO_2 nano-composite electrodes from PSS dispersed MWCNTs. PSS functions as an effective dispersant for MWCNTs and provides the surface functionalities ($-SO_3^-$) as charged sites that facilitate an ordered growth of active materials on MWCNTs. In-situ oxidation of pyrrole with $KMnO_4$ yields molecular level dispersion of MnO_2 in PPy matrix that improves the electronic conductivity, mechanical stability and pseudo-capacitance. The improved electrical conduction in MWCNT-PSS/PPy:MnO_2 nano-composite resulted in high specific capacitance, excellent rate capability and the long cycling life stability over 5000 cycles.

Acknowledgements

We thank Dr. Diego Diaz and Anindarupa Chunder for their valuable suggestions. Characterization support from Material Characterization Facility at the University of Central Florida and the financial support from National Science Foundation CAREER award DMR 0746499 are gratefully acknowledged.

References

[1] P. Simon, Y. Gogotsi, Nat. Mater. 7 (2008) 845–854.
[2] T. Brousse, M. Toupin, R. Dugas, L. Athouel, O. Crosnier, D. Bélanger, J. Electrochem. Soc. 153 (2006) A2171–A2180.
[3] M. Toupin, T. Brousse, D. Bélanger, Chem. Mater. 16 (2004) 3184–3190.
[4] B.E. Conway, V. Birss, J. Wojtowicz, J. Power Sources 66 (1997) 1–14.
[5] M. Mastragostino, C. Arbizzani, F. Soavi, J. Power Sources 97 (98) (2001) 812–815.
[6] V. Subramanian, H. Zhu, B. Wei, Electrochem. Commun. 8 (2006) 827–832.
[7] R.K. Sharma, H.S. Oh, Y.G. Shul, H.S. Kim, J. Power Sources 173 (2007) 1024–1028.
[8] H.A. Andreas, B.E. Conway, Electrochim. Acta 51 (2006) 6510–6520.
[9] C.C. Hu, T.W. Tsou, Electrochem. Commun. 4 (2002) 105–109.
[10] C. Niu, E.K. Sichel, R. Hoch, D. Moy, H. Tennent, Appl. Phys. Lett. 70 (1997) 1480–1482.
[11] E.R. Pinero, V. Khomenko, E. Frackowaik, F. Béguin, J. Electrochem. Soc. 152 (2005) A229–A235.
[12] S.-L. Chou, J.-Z. Wang, S.-Y. Chew, H.-K. Liu, S.-X. Dou, Electrochem. Commun. 10 (2008) 1724–1727.
[13] C. Peng, S. Zhang, D. Jewell, G.Z. Chen, Prog. Nat. Sci. 18 (2008) 777–788.
[14] O.-K. Park, T. Jeevananda, N.-H. Kim, S-il Kim, J.-H. Lee, Scripta Mater. 60 (2009) 551–554.
[15] C. Meng, C. Liu, S. Fan, Electrochem. Commun. 11 (2009) 186–189.
[16] R.K. Sharma, L. Zhai, Electrochim. Acta 54 (2009) 7148–7155.
[17] H. Zhang, G. Cao, Z. Wang, Y. Yang, Z. Shib, Z. Gub, Electrochem. Commun. 10 (2008) 1056–1059.
[18] C. Duarte, M.A. Sobal, N.L. Marzan, L.M. Giersig, Adv. Mater. 16 (2004) 2179–2184.
[19] D. Briggs, M.P. Seah, Practical Surface Analysis, Wiley, New York, 1990, Appendix 6, p. 6355.
[20] M. Chigane, M. Ishikawa, J. Electrochem. Soc. 147 (2000) 2246–2251.
[21] B.J. Tan, B.J. Klabunde, P.M.A. Sherwood, J. Am. Chem. Soc. 113 (1991) 855–861.
[22] M. Chigane, M. Ishikawa, M. Izaki, J. Electrochem. Soc. 148 (2001) D96–D101.
[23] M. Kruk, M. Jaroniec, Chem. Mater. 13 (2001) 3169–3183.
[24] J. Joo, J.K. Lee, K.S. Jang, E.J. Oh, A.J. Epstein, Macromolecules 33 (2000) 5131.
[25] R.K. Sharma, A.C. Rastogi, S.B. Desu, Electrochem. Commun. 10 (2008) 268–272.